Monitoring Chlorophyll-a Concentration of Gorgan Bay, Southeastern Caspian Sea, using Sentinel-2 Data

Salar Khani [1], Ata A. Kakroodi [1,*], Sara Attarchi [1]

Department of Remote Sensing and GIS, University of Tehran, P.O. Box 14155-4665, Tehran, Iran

Keywords: Gorgan Bay, Water Quality, Satellite Data, Random Forest, Classification and Regression Tree, Gradient Tree Boost.

Abstract

Gorgan Bay, a vital ecological and economic region in the southeastern Caspian Sea, faces escalating threats from climate change and human activities, resulting in diminished water volume and deteriorating quality. This study harnesses cutting-edge machine learning and remote sensing to monitor chlorophyll-a (Chl-a) concentrations, a key indicator of water quality and ecosystem health. Leveraging Sentinel-2 satellite data, field measurements, and advanced regression models, we explored correlations between spectral bands, the Normalized Difference Chlorophyll Index (NDCI), and water depth to predict Chl-a levels. Multiple linear regression (MLR), Random Forest (RF), Classification and Regression Trees (CART), and Gradient Tree Boost (GTB) models were developed to map Chl-a distributions, with various input combinations rigorously tested. The CART model emerged as the top performer, achieving a Root Mean Squared Error (RMSE) of 6.32 µg/L and a coefficient of determination (R^2) of 0.82, demonstrating robust predictive accuracy. These findings offer a powerful tool for real-time monitoring of Gorgan Bay's ecological status, providing critical insights for conservation strategies and sustainable management. By integrating satellite technology with machine learning, this research paves the way for innovative approaches to safeguard vulnerable aquatic ecosystems, captivating researchers and policymakers eager to address pressing environmental challenges.

1. Introduction

Over the past few decades, there has been a consistent decline in water resources and deterioration in water quality in many parts of the world. Water pollution has emerged as a complex and pressing issue that threatens the economic and developmental policies of many countries (Han et al., 2016).

Various factors within a water body, such as the influx of pollutants and sediments from rivers, agricultural runoff, and the point-source introduction of industrial pollutants can contribute to temporal changes in water quality (Ranjbar and Hadjizadeh-Zaker, 2016). Additionally, the environmental conditions of the water body, including flow patterns, geographical location, climatic factors such as wind speed and precipitation, and the geometric and hydrological characteristics of inlet and outlet channels, can determine the spatial distribution patterns of suspended or dissolved substances in the water. To protect water resources, acquiring comprehensive data on both pollutant distribution across water bodies and temporal variations in water quality parameters is of paramount importance (Sun et al., 2022).

The main objective of water quality monitoring is to ensure the safety of human health and the environment, as well as to assess the impact on economic activities dependent on water resources (González-Marcuaz et al., 2018). Monitoring water quality and understanding the physical, chemical, and biological conditions of aquatic environments are of critical importance to both researchers and policymakers.

Conventional approaches to water quality monitoring rely on field measurements using specialized instruments or the collection and laboratory analysis of samples to determine the physical, chemical, and biological properties of water. These measurements are typically conducted at specific, limited locations and may not be performed at consistent time intervals. Traditional water quality monitoring methods are constrained in terms of both spatial coverage and sampling frequency. In recent years, the availability of satellite data, progress in image processing software, and the advancement of empirical, mathematical, and machine learning models have transformed remote sensing into an effective tool for evaluating water quality. This is achieved by leveraging the relationship between electromagnetic waves and water molecules and their constituents (Casal and Lavender, 2017).

Given the unique capabilities provided by remote sensing, in recent years, multi-temporal satellite imagery, such as Landsat and Sentinel, has been employed in coastal areas, seas, and lakes to investigate water quality indicators, including dissolved organic matter, turbidity, salinity, and chlorophyll-a concentrations, on both regional and global scales. Fluctuations in water quality result in changes in the optical characteristics of water (Pavelsky and Smith, 2009). This principle underpins recent studies that have focused on developing empirical models to estimate water quality by correlating in situ or laboratory-measured values with reflectance data derived from satellite imagery. By employing regression models and calculating mathematical relationships between spectral reflectance bands and field data, it is possible to predict most water quality indicators (Seenipandi et al., 2021). This approach enables mapping the spatial distribution of water quality parameters across the entire study area, rather than being restricted to measurements at ground-based stations only. This method facilitates a deeper understanding of the spatial distribution of these parameters, offering valuable near-real-time information to water resource and environmental managers to support decision-making based on the region's actual conditions.

* Corresponding author: a.a.kakroodi@ut.ac.ir

This contribution has been peer-reviewed. The double-blind peer-review was conducted on the basis of the full paper.
https://doi.org/10.5194/isprs-annals-X-4-W8-2025-433-2026 | © Author(s) 2026. CC BY 4.0 License.

One of the most significant indicators of water quality in a water body is chlorophyll concentration. Chlorophyll is a photosynthetically active substance that transforms light into energy for photosynthesis. Chlorophyll-a (Chl-a), the most abundant form of chlorophyll (Topp et al., 2020), acts as an indicator of plankton distribution in water and serves as the primary index for evaluating the organic matter produced by photosynthetic organisms and the trophic state (eutrophication) of aquatic ecosystems (Yang et al., 2022). Eutrophication refers to the enrichment of water with nutrients, leading to excessive algal growth and algal blooms. Consequently, monitoring Chl-a concentrations and predicting algal blooms in advance are critical. The concentration of Chl-a is typically measured and reported in units of grams per cubic meter (g/m³) or micrograms per liter (µg/L), which are equivalent units.

In the past two decades, multispectral and hyperspectral data have been used to estimate Chl-a concentrations. Chl-a absorbs photons predominantly in blue and red wavelengths, while reflecting photons in the green range (Rawat et al., 2023). This unique spectral response forms the basis for deriving the Normalized Difference Chlorophyll Index (NDCI). Reflectance values from red and near-infrared bands are frequently used to generate NDCI (Rawat et al., 2023; Dabire et al., 2024).

Recent studies have employed satellite data and machine learning approaches to monitor Chl-a concentrations in the water. Chebud et al. (2012) applied Landsat 5 data with an artificial neural network (ANN) model to estimate Chl-a, turbidity, and phosphorus. Hafeez et al. (2019) used Landsat 5, 7, and 8 images with random forest (RF), support vector regression (SVR), ANN, and Cubist methods to assess coastal water quality in Hong Kong, with ANN yielding the highest accuracy. Wang et al. (2020) developed a support vector machine (SVM) model in Google Earth Engine (GEE) to accurately predict Chl-a in Ohio lakes. Peterson et al. (2020) employed multiple-linear regression (MLR), SVR, extreme learning regression (ELR), and deep learning (DL) with Landsat 8 and Sentinel-2 data, achieving low-error predictions. Leggesse et al. (2023) compared various regression models and found out that extreme gradient boosting (XGBoost) and RF were the most accurate techniques for estimating Chl-a and turbidity, respectively.

Kazempour et al. (2023) mapped monthly Chl-a in Gorgan Bay during 2020–2021 using a Sentinel-2-driven ANN (R^2 = 0.88, RMSE = 1.51 mg/m³), revealing persistent high-concentration zones in the southeast near the Qarasu River outlet. Maleki et al. (2024) reported seasonal-spatial water quality variability in Gorgan Bay, driven by nutrient fluxes and limited Caspian exchange. Beal et al. (2024) utilized Sentinel-2 and Sentinel-3 imagery to estimate Chl-a concentrations in Lake Mendota, Madison, USA. The predictive model attained an R^2 of 0.47, with the highest accuracy obtained using the Sentinel-2 data. Wu et al. (2025) developed PC-STDM to downscale Sentinel-2 Chl-a to hourly resolution using GOCI data (R^2=0.87), enabling detailed eutrophication monitoring in Taihu Lake. Astiti et al. (2025) mapped Chl-a and TSM in southeast Bali using Sentinel-2 imagery, finding peak Chl-a (43.65 mg/m³) in the rainy season and TSM (42.77 mg/L) during the dry-to-rainy transition. Zhao and O'Loughlin (2025) monitored Chl-a concentrations in Irish lakes using Landsat 8, Sentinel-2, and MODIS data with RF, SVM, and XGBoost models. The RF model, paired with MODIS data, provided the highest accuracy, with an R^2 of 0.595. Assaf et al. (2025) used Sentinel-2 images and XGBoost, ridge regression (RR), ANN, CatBoost, RF, and SVR to estimate Chl-a in small-scale semi-arid reservoirs. The RF model outperformed the others, achieving an R^2 of 0.91.

The literature review indicates that machine learning methods demonstrate strong performance in estimating water quality parameters, including Chl-a. The objective of our study was to estimate the Chl-a concentration in Gorgan Bay, southeastern Caspian Sea. For this purpose, four different regression techniques were used to retrieve Chl-a from the Sentinel-2 data. The accuracy of the models was tested using various performance metrics.

2. Study Area and Data

1.1 Study Area

Gorgan Bay, the largest bay along the Caspian Sea, is situated in the southeastern region of the sea, within the geographical coordinates of 53°25' to 54°6' East longitude and 36°46' to 37°0' North latitude (Gharibreza et al., 2018). The bay is linked to the Caspian Sea via the Ashuradeh Channel. The average depth of the bay is less than 1.5 m, with a maximum depth of 6.5 m, increasing from west to east and toward the southern areas of Ashuradeh Island. The bay encompasses an area of approximately 400 km², with a maximum length of 70 km (Kheirabadi et al., 2018).

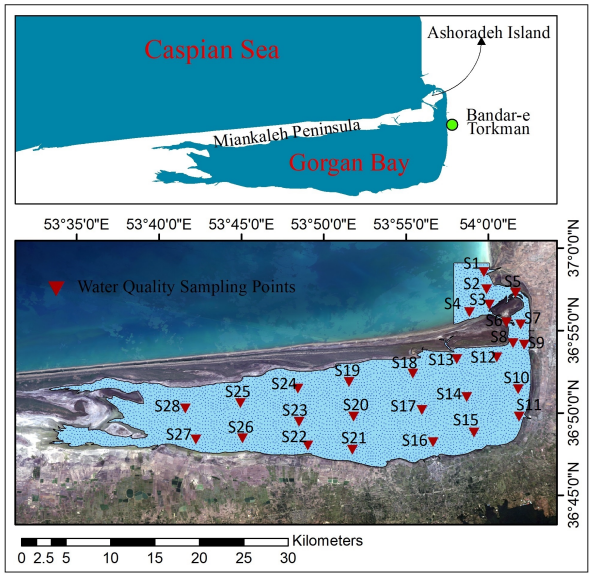

Figure 1. Gorgan Bay and water quality sampling locations.

Gorgan Bay is characterized by its substantial ecosystem diversity and was one of the first wetlands designated under the Ramsar Convention in 1975. Furthermore, in 1976, it was designated by UNESCO as one of the nine biosphere reserves. Figure (1) illustrates the study area and water quality sampling points.

1.2 Field Data

In this study, to estimate the Chl-a concentrations of Gorgan Bay, recorded data from the bay were utilized for training and developing machine learning models, as well as evaluating their performance. The data were recorded by the Iranian National Institute for Oceanography and Atmospheric Science on September 13, 2020, and included measurements of Chl-a and

maximum depth at 28 stations across Gorgan Bay, the connecting channel to the Caspian Sea, and a portion of the Caspian Sea at the junction with Gorgan Bay. The spatial distribution of these stations throughout the region is adequate, encompassing nearly all areas with varying water depths and the coastal and interior zones of Gorgan Bay. The locations of the sampling points are shown in Figure (1).

1.3 Satellite Data

In this study, Sentinel-2 image at the field sampling date was employed to extract the Chl-a concentration over Gorgan Bay. Figure (2) shows a false-colour composite of the satellite image. Sentinel-2 is a multispectral imaging mission with a wide swath and 5-day global revisit frequency. The Sentinel-2 Multispectral Instrument (MSI) records data across 13 spectral bands, including visible and near-infrared (NIR) at 10-meter resolution, red-edge and shortwave infrared (SWIR) at 20-meter resolution, and atmospheric bands at 60-meter spatial resolution. This instrument delivers suitable information for studying the status and changes in water, soil, and vegetation. Surface reflectance data from Sentinel-2 have been available to researchers since March 2017.

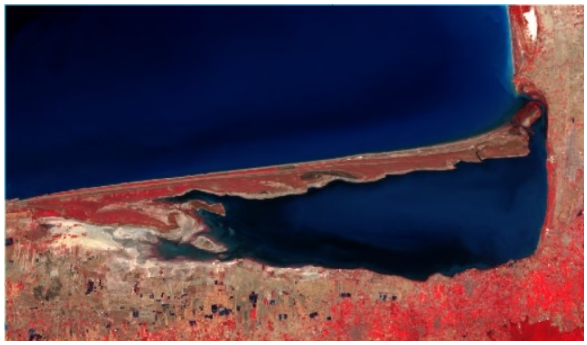

Figure 2. The false color composite of the Sentinel-2 image obtained for September 13, 2020.

3. Methodology

3.1. Methods

In this study, four methods were employed to determine the Chl-a concentration in Gorgan Bay: multiple linear regression (MLR), random forest (RF), classification and regression tree (CART), and gradient tree boost (GTB). In the following sections, a brief description of each model is provided.

MLR is one of the most commonly applied methods for estimating water quality parameters. This model predicts parameter values as a linear function of one or more independent variables, incorporating an error term (Khani and Khademi-Shiraz, 2024). The MLR model relies on the least-squares approach, whereby the model is adjusted to reduce total of squared discrepancies between the measured and estimated values.

CART models generate decision trees through optimal node splits based on various criteria, enabling classification or continuous value predictions. Initially introduced by Breiman et al. (1984), this approach serves as the foundation for many modern tree-based methods and is widely applied in geographical analysis and big data processing. The CART model constructs a simple decision tree by recursively splitting the data into two sequential groups at the initial nodes to maximize output symmetry. For regression, the objective is to minimize the squared error between the estimated and measured values (Breiman et al., 1984). In regression problems, the output of each node is the mean of the sample labels within that node, with splitting decisions based on error metrics like Mean Squared Error (MSE).

The RF method, developed by Breiman (2001), is used for classification and regression. It comprises an ensemble of decision trees, where each tree votes for the class assigned to a specific sample, and the most frequent response determines the outcome (Gómez et al., 2021). For regression, the output is the average of the trees' predictions.

The GTB model, which is part of the boosting family, progressively constructs stronger models by combining the distributed weaknesses of the base models. This approach is particularly effective for regression tasks and is relatively resistant to overfitting because of its ability to manage model complexity and reduce variance. The boosting process enhances efficiency by utilizing outputs from previous models to train subsequent models, thereby reducing the model size and prediction time. This model has recently gained widespread use owing to its high precision, rapid training and prediction speed, and low memory usage (Si et al., 2017).

3.2. Statistical Analysis of the Data

Table (1) summarizes the results of the statistical analysis of the field data. Based on the statistical analysis, the maximum depth of the sampling points was 3 m at station 19. The minimum and maximum Chl-a values were observed at stations 27 and 12, respectively. Based on the results of the statistical analysis of the data during field data collection, the lowest Chl-a value was 1.06 µg/L, and its highest concentration was 42.10 µg/L.

Statistical Parameter	Chl-a (µg/L)	Depth (m)
Min	1.06	0.20
Max	42.10	3.00
Median	13.61	1.48
Mean	14.83	1.54
S_d	11.466	0.802

Table 1. Descriptive statistics of the data

3.3. Extracting Chl-a from Sentinel-2 Image

In this study, atmospherically corrected surface reflectance data from Sentinel-2, accessed via the Google Earth Engine (GEE) platform, were used to monitor the Chl-a concentration in Gorgan Bay. From the 28 recorded data points, 20 data points, equivalent to 70% of the dataset, were employed to train the machine learning algorithms, whereas the remaining 8 data points, representing 30% of the data, were utilized to evaluate the models' performance. A correlation of 0.494 was observed between water depth and Chl-a levels. Consequently, water depth data were also used to estimate this water quality parameter. In the first step, the Chl-a training data and bay depth data were used to generate the corresponding raster data using the inverse distance weighting (IDW) interpolation method in ArcMap, serving as the target and input parameters during the model training phase, respectively. While the use of interpolated Chl-a and depth data introduces potential sources of error in modeling, it can be justified given the high cost of field measurements and the need to enhance the speed of water quality monitoring. Moreover, this approach enables the use of

an increased number of input data points, improves the training of machine learning models, and increases their generalizability.

Sentinel-2 bands' reflectance values were utilized individually and in combination with other bands as input variables for the Chl-a predictive models. Subsequently, various regression models were applied to establish the relationship between field-measured Chl-a concentrations and Sentinel-2 surface reflectance data. Following this, distribution maps of Chl-a across Gorgan Bay were generated for each model. Finally, the accuracies of these models were assessed against the test data using performance measures. Figure (3) depicts the workflow employed for the extraction of Chl-a concentration from Sentinel-2 image.

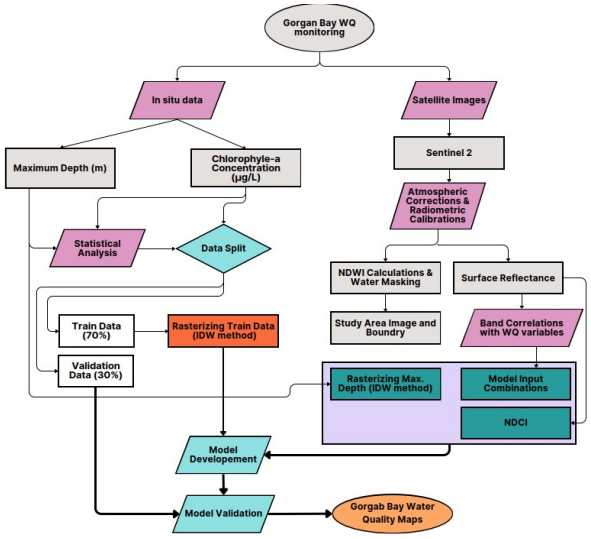

Figure 3. Workflow for extracting Chl-a concentration of Gorgan Bay from Sentinel-2 data.

3.4. Model Inputs

Initially, the correlation between the surface reflectance of various bands of the Sentinel-2 image and the actual Chl-a concentrations measured across Gorgan Bay was calculated, with the results presented in Table (2). Subsequently, the effective bands were selected based on their highest absolute correlation values and were utilized individually and in combination with other bands to create four distinct band combinations (C1—C4), which served as inputs for the models.

In addition to these band combinations, the NDCI was calculated for Gorgan Bay and used both independently and in conjunction with the initial band combinations as the model inputs (input combinations C5 to C9). The NDCI was calculated from the reflectance in the red and NIR bands of the image using Equation (1). To investigate the influence of water depth on Chl-a concentrations, bay depth data were used independently and alongside the initial band combinations for Chl-a estimation (input combinations C10 to C14). The details of these 14 input combinations are provided in Table (3), and the interpolated depth map of Gorgan Bay is shown in Figure (4).

Band	Band Description	Correlations with Chl-a
B1	Aerosols	0.04
B2	Blue	0.18
B3	Green	0.44
B4	Red	0.21
B5	Red Edge 1	0.32
B6	Red Edge 2	0.07
B7	Red Edge 3	0.02
B8	NIR	-0.04
B8A	Red Edge 4	-0.09
B9	Water vapor	-0.38
B11	SWIR 1	-0.27
B12	SWIR 2	-0.35

Table 2. Calculated correlation coefficients between Chl-a and the surface reflectance of the Sentinel-2 bands

$$NDCI = \frac{Red-NIR}{Red+NIR}, \quad (1)$$

where Red = red band reflectance
NIR = near-infrared band reflectance

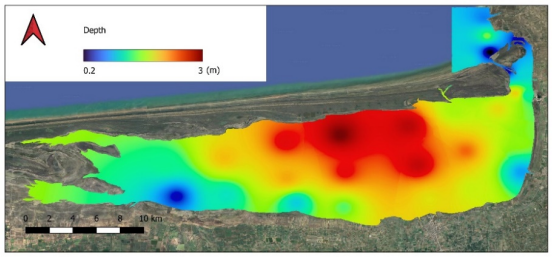

Figure 4. The depth map of Gorgan Bay.

Input Combinations	Input Parameters
C1	B3
C2	B3 & B9
C3	B3, B9 & B12
C4	B3, B5, B9 & B12
C5	NDCI
C6	NDCI & C1
C7	NDCI & C2
C8	NDCI & C3
C9	NDCI & C4
C10	Depth
C11	Depth & C1
C12	Depth & C2
C13	Depth & C3
C14	Depth & C4

Table 3. Input combinations for the models to estimate Chl-a.

3.5. Models' Performance Metrics

The performance of the models was evalueted employing various performance criteria, including the coefficient of determination (R^2), Nash-Sutcliffe Efficiency (NSE), Root Mean Square Error (RMSE), Mean Absolute Error (MAE), Ratio of predicted to observed values (R_{ratio}), and Mean Absolute Percentage Error (MAPE). R^2 and NSE, ranging from 0 to +1 and -∞ to +1, respectively, evaluate the goodness of fit, with +1 indicating optimal model performance. The RMSE and MAE measure prediction errors, with values near zero reflecting higher accuracy. R_{ratio} assesses the over- or underestimation by the models. MAPE, which ranges from 0 to ∞, quantifies the average percentage error, with lower values indicating better precision. Together, these metrics offer a thorough assessment of the model performance in estimating Chl-a concentrations.

$$R^2 = \frac{\sum_{i=1}^{n}\left(WQ_{i(estimated)} - WQ_{i(mean)}\right)^2}{\sum_{i=1}^{n}\left(WQ_{i(observed)} - WQ_{i(mean)}\right)^2}, \quad (1)$$

$$NSE = 1 - \frac{\sum_{i=1}^{n}\left(WQ_{i(observed)} - WQ_{i(estimated)}\right)^2}{\sum_{i=1}^{n}\left(WQ_{i(observed)} - WQ_{i(mean)}\right)^2}, \quad (2)$$

$$RMSE = \sqrt{\frac{\sum_{i=1}^{n}\left(WQ_{i(observed)} - WQ_{i(estimated)}\right)^2}{n}}, \quad (3)$$

$$MAE = \frac{\sum_{i=1}^{n}\left|WQ_{i(observed)} \;\; WQ_{i(estimated)}\right|}{n}, \quad (4)$$

$$R_{ratio} = \frac{\sum_{i=1}^{n} WQ_{i(estimated)}}{\sum_{i=1}^{n} WQ_{i(observed)}}, \quad (5)$$

$$MAPE = \frac{100}{n} \times \sum_{i=1}^{n}\left|\frac{WQ_{i(observed)} - WQ_{i(estimated)}}{WQ_{i(observed)}}\right|, \quad (6)$$

where n = number of test samples
$WQ_{i(mean)}$ = mean value of observed Chl-a
$WQ_{i(observed)}$ = observed Chl-a
$WQ_{i(estimated)}$ = estimated Chl-a

4. Results and Discussion

The MLR model was employed to estimate Chl-a levels using 14 different input combinations of C1 to C14. For each input data, the regression equation along with the RMSE and R^2 values are summarized in Table (4). The highest accuracy for the MLR method was achieved with combination C13, which included the water depth variable, yielding an RMSE of 8.66 µg/L and an R^2 of 0.51. The NDCI index, when used independently as an input for the MLR model (C5), exhibited the lowest level of accuracy. The estimation accuracy of Chl-a based solely on depth (C10) was nearly comparable to that using Sentinel-2 single bands; however, the highest MLR accuracy was obtained when depth was combined with Sentinel-2 bands (combinations C11 to C14).

The RF, CART, and GTB models were also applied using input combinations C1 to C9, which included the surface reflectance of various bands and the NDCI index, to estimate Chl-a concentrations. The best results of the models are summarized in Table (5). The RF, CART, and GTB models achieved their greatest accuracy when the NDCI was used alongside the bands as the model input. The highest accuracies of the RF and GTB models were achieved using C6 inputs containing the NDCI and green band reflectance values. The CART model provided the best estimations of Chl-a for C8 inputs, including the reflectance of the green, watervapor, and SWIR2 bands and NDCI values.

Input	Regression Equation	R^2	RMSE
C1	3.91+(116.37×Green)	0.27	9.85
C2	4.71+(119.80×Green) -(66.77×Watervapor)	0.31	9.71
C3	4.83+(119.44×Green) -(89.01×Watervapor)+(26.98×SWIR2)	0.31	9.71
C4	5.09+(141.38×Green) -(52.90×RedEdge1) -(54.25×Watervapor)+(34.73×SWIR2)	0.31	9.73
C5	14.37+(1.71×NDCI)	0.19	11.11
C6	2.87+(124.88×Green)+(15.31×NDCI)	0.38	9.50
C7	3.63+(132.23×Green) -(90.35×Watervapor)+(20.17×NDCI)	0.45	9.21
C8	3.85+(131.88×Green) -(136.66×Watervapor)+(55.27×SWIR2) +(20.82×NDCI)	0.46	9.19
C9	3.51+(227.98×Green) -(193.25×RedEdge1) -(70.82×Watervapor)+(119.86×SWIR2) +(47.54×NDCI)	0.68	8.67
C10	3.85+(5.97×Depth)	0.31	9.72
C11	-2.84+(95.95×Green)+(4.87×Depth)	0.50	8.72
C12	-2.29+(98.05×Green) -(29.56×Watervapor)+(4.72×Depth)	0.51	8.67
C13	-2.20+(97.85×Green) -(43.67×Watervapor)+(17.07×SWIR2) +(4.72×Depth)	0.51	8.66
C14	-1.97+(107.16×Green) -(30.40×Watervapor)+(20.43×SWIR2) -(21.45×RedEdge1)+(4.63×Depth)	0.51	8.69

Table 4. Regression equations obtained for estimating Chl-a

Among the four methods, the GTB model exhibited the lowest accuracy with an RMSE of 10.39 µg/L. The RF and CART models demonstrated better performance in estimating Chl-a concentrations than the other two methods, with the CART model achieving the highest accuracy, recording an RMSE of 6.32 µg/L and an R^2 of 0.82. Additionally, the NSE coefficient for this model was calculated as 0.67, and its R_{ratio} was 1.01, indicating a good fit and estimates closely aligned with the actual values.

Model	MLR	RF	CART	GTB
Inputs	C13	C6	C8	C6
R^2	0.51	0.83	0.82	0.66
NSE	0.38	0.54	0.67	0.11
MAE	7.53	6.99	5.38	9.79
RMSE	8.66	7.47	6.32	10.39
R_{ratio}	0.85	0.91	1.01	0.89
MAPE	128.61	145.33	143.12	199.48

Table 5. Performance of the models for estimating Chl-a

Figure (5) displays scatter plots comparing the estimated Chl-a concentrations derived from Sentinel-2 band combinations, the NDCI index, and water depth against actual Chl-a values at test stations using the MLR, RF, CART, and GTB methods. The superior performance of the RF and CART models and the weaker performance of the GTB model can be inferred from these plots.

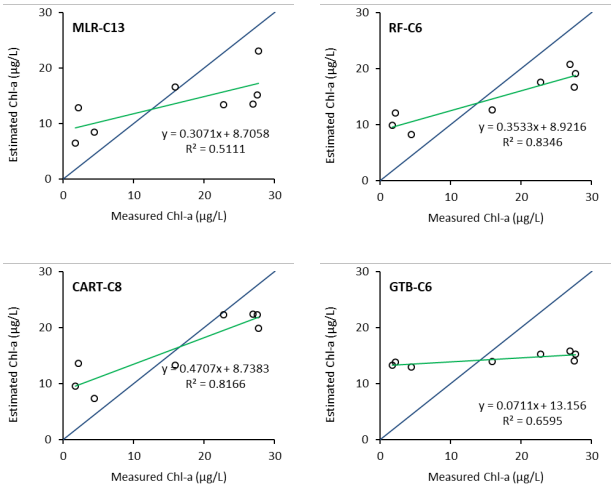

Figure 5. Scatter plots of estimated versus measured Chl-a.

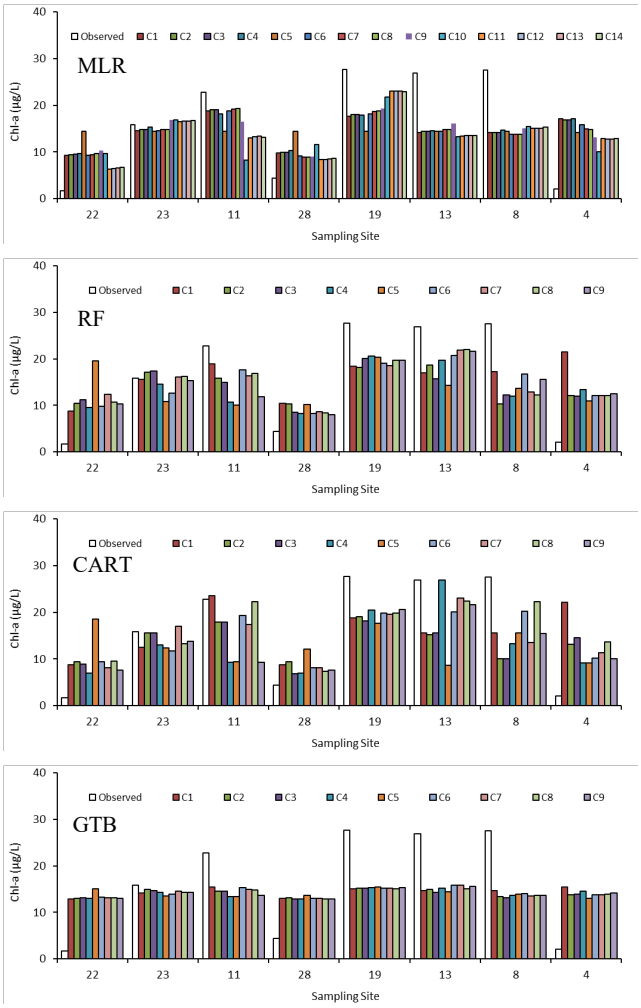

Figure 6. Performance of the models in estimating Chl-a concentrations at test stations

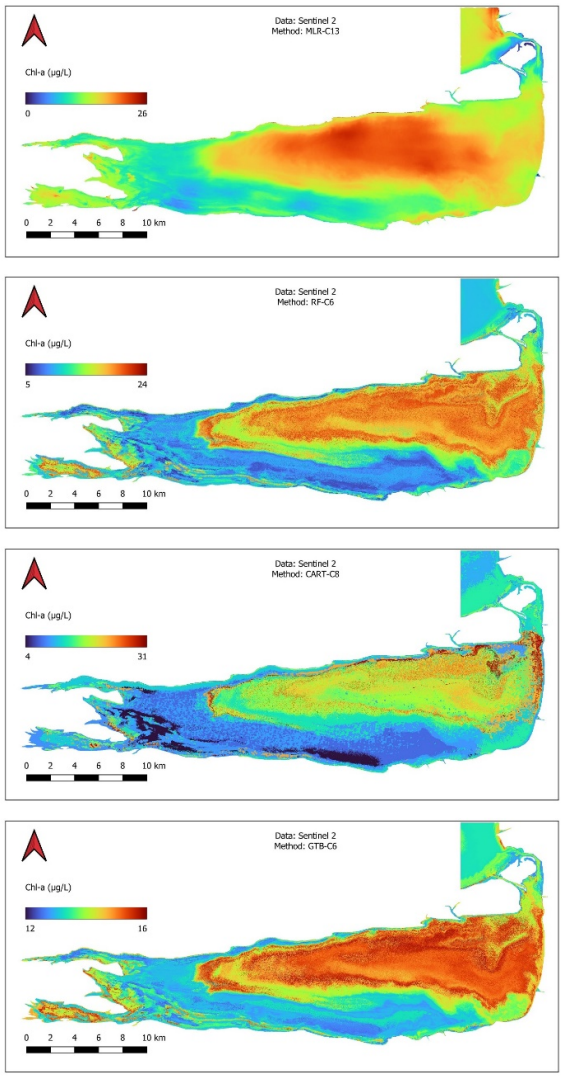

Figure 7. Chl-a distribution maps obtained from the most accurate MLR, RF, CART, and GTB models.

To assess the accuracy of the models in estimating Chl-a concentrations at the test stations and evaluate their performance in predicting the lower and upper limits of this water quality variable, the estimated Chl-a values from all the four models using various input combinations are presented in Figure (6). While none of the models provided acceptable performance in estimating low Chl-a values at stations 4 and 22, the higher concentrations at stations 8, 13, and 19 were more accurately predicted by the CART model than by the other three models.

The results of the MLR, RF, CART, and GTB models are presented as Chl-a concentration distribution maps in Figure (7). The distribution patterns of Chl-a in Gorgan Bay were broadly similar across all methods. The concentration of this water quality parameter increased from west to east. The RF and CART results indicated that the Chl-a levels at the junction of the Caspian Sea with Gorgan Bay were lower than those within the bay. The Chl-a minimum and maximum ranges were close for the MLR, RF, and CART models. However, the Chl-a estimations by the GTB model were in the range of 12-16 µg/L, indicating the poor performance of this model.

5. Conclusion

To monitor Gorgan Bay Chl-a concentrations, the MLR, RF, CART, and GTB methods were employed. The input variables for these models included various combinations of effective bands from Sentinel-2, along with the calculated NDCI and water depth of the bay. The statistical analysis of Chl-a data revealed that this water quality parameter varied between 1.06 µg/L and 42.10 µg/L across field measurement stations. The lowest value was recorded at station 27 in the western part of Gorgan Bay, while the highest was observed at station 12 in the east, near the confluence of the Qarasu River. Elevated Chl-a levels in this region may indicate an accumulation of nutrients, such as phosphorus and nitrate, which are transported into the Gorgan Bay via this river. The origin of these nutrients is likely attributable to anthropogenic activities, including agriculture, the application of chemical fertilizers, or wastewater discharge. This nutrient enrichment can lead to reduced dissolved oxygen levels in the water (hypoxia) due to algal decomposition, resulting in adverse impacts on both faunal and floral species.

This contribution has been peer-reviewed. The double-blind peer-review was conducted on the basis of the full paper.
https://doi.org/10.5194/isprs-annals-X-4-W8-2025-433-2026 | © Author(s) 2026. CC BY 4.0 License.

The correlation between Chl-a and water depth data was calculated as 0.494. Results of the MLR model reveal that the bay depth data alongside the surface reflectance of the satellite image results higher accuracies for Chl-a estimation. The modeling results indicated that the CART model, utilizing Sentinel-2 data, achieved the highest performance in estimating Chl-a concentrations, with an RMSE of 6.32 µg/L and an R^2 of 0.82. Additionally, this water quality parameter's spatial distribution map showed an increasing trend from west to east across Gorgan Bay, consistent with field measurements. Furthermore, it was concluded that the GTB model exhibited the lowest accuracy in estimating Chl-a values.

Previous studies for estimating Chl-a by Leggesse et al. (2023), Beal et al. (2024), Assaf et al. (2025), and Zhao and O'Loughlin (2025) reported R^2 accuracies of 0.78 (XGBoost), 0.47 (Sentinel-2 data), 0.91 (RF with Sentinel-2), and 0.595 (RF with MODIS), respectively. In the current study, the CART model, with an R^2 of 0.82, was identified as the most accurate model for estimating Chl-a in Gorgan Bay, outperforming the results of Legesse et al. (2023), Beal et al. (2024), and Zhao and O'Loughlin (2025).

To estimate Chl-a concentrations and generate distribution maps for this water quality parameter, 41 modeling stages were conducted using four different models with various input data, including combinations of Sentinel-2 effective bands, the bay depth data, and the NDCI index. The results demonstrated that using different Sentinel-2 bands can provide suitable accuracy in extracting Chl-a for this bay. Additionally, the performance of the machine learning models highlighted their effectiveness in estimating this parameter with minimal error.

References

Assaf, M.N., Abdelal, Q., Hussein, N.M., Halaweh, G., Alzubaidi, A.J., 2025. Water quality monitoring and management: integration of machine learning algorithms and Sentinel-2 images for the estimation of Chlorophyll-a. *Modeling Earth Systems and Environment*, *11*(5), pp.1-26.

Astiti, S. P. C., Dharma, I. G. B. S., Pariartha, I. P. G. S., As-Syakur, A. R., Arsana, I. G. N. K., 2025. Analysis of total suspended matter and chlorophyll-a in southeast Bali using Sentinel-2 satellite imagery data. *Ecological Engineering & Environmental Technology*, *26*(7), 152-166.

Beal, M.R., Özdoğan, M., Block, P.J., 2024. A machine learning and remote sensing-based model for algae pigment and dissolved oxygen retrieval on a small inland lake. *Water Resources Research*, *60*(3), p.e2023WR035744.

Breiman, L., 2001. Random forests. *Machine learning*, *45*(1), pp.5-32.

Breiman, L., Friedman, J., Olshen, R.A., Stone, C.J., 2017. *Classification and regression trees*. Chapman and Hall/CRC.

Casal, G., Lavender, S., 2017. Spatio-temporal variability of sea surface temperature in Irish waters (1982–2015) using AVHRR sensor. *Journal of sea research*, *129*, pp.89-104.

Chebud, Y., Naja, G.M., Rivero, R.G., Melesse, A.M., 2012. Water quality monitoring using remote sensing and an artificial neural network. *Water, Air, & Soil Pollution*, *223*(8), pp.4875-4887.

Dabire, N., Ezin, E.C., Firmin, A.M., 2024. Water Quality Assessment Using Normalized Difference Index by Applying Remote Sensing Techniques: Case of Lake Nokoue. In *2024 IEEE 15th Control and System Graduate Research Colloquium (ICSGRC)* (pp. 1-6). IEEE (August 2024).

Gharibreza, M., Nasrollahi, A., Afshar, A., Amini, A., Eisaei, H., 2018. Evolutionary trend of the Gorgan Bay (southeastern Caspian Sea) during and post the last Caspian Sea level rise. *Catena*, *166*, pp.339-348.

Gómez, D., Salvador, P., Sanz, J., Casanova, J.L., 2021. A new approach to monitor water quality in the Menor sea (Spain) using satellite data and machine learning methods. *Environmental Pollution*, *286*, p.117489.

González-Márquez, L.C., Torres-Bejarano, F.M., Rodríguez-Cuevas, C., Torregroza-Espinosa, A.C., Sandoval-Romero, J.A., 2018. Estimation of water quality parameters using Landsat 8 images: application to Playa Colorada Bay, Sinaloa, Mexico. *Applied Geomatics*, *10*(2), pp.147-158.

Hafeez, S., Wong, M.S., Ho, H.C., Nazeer, M., Nichol, J., Abbas, S., Tang, D., Lee, K.H., Pun, L., 2019. Comparison of machine learning algorithms for retrieval of water quality indicators in case-II waters: A case study of Hong Kong. *Remote sensing*, *11*(6), p.617.

Han, D., Currell, M.J., Cao, G., 2016. Deep challenges for China's war on water pollution. *Environmental Pollution*, *218*, pp.1222-1233.

Kazempour, Z., Danesh-Yazdi, M., Asadifakhr, K., Raie, M., 2023. Spatiotemporal dynamics of chlorophyll-a in the Gorgan Bay and Miankaleh Peninsula biosphere reserve: Call for action. *Remote Sensing Applications: Society and Environment*, *30*, 100946.

Khani, S., Shiraz, N.K., 2024. Electrical Conductivity Estimation in the Medina River, Texas, USA: An Integrated Approach Using Wavelet Analysis and Machine Learning Techniques. In *River Basin Management-Challenges and Coping Strategies*. IntechOpen.

Kheirabadi, H., Noori, R., Samani, J.M., Adamowski, J.F., Ranjbar, M.H., Zaker, N.H., 2018. A reduced-order model for the regeneration of surface currents in Gorgan Bay, Iran. *Journal of Hydroinformatics*, *20*(6), pp.1419-1435.

Kutser, T., 2009. Passive optical remote sensing of cyanobacteria and other intense phytoplankton blooms in coastal and inland waters. *International Journal of Remote Sensing*, *30*(17), pp.4401-4425.

Leggesse, E.S., Zimale, F.A., Sultan, D., Enku, T., Srinivasan, R., Tilahun, S.A., 2023. Predicting optical water quality indicators from remote sensing using machine learning algorithms in tropical highlands of Ethiopia. *Hydrology*, *10*(5), p.110.

Maleki, P., Rahman, P., Jafaryan, H., Salmanmahiny, A., Ghorbani, R., Gholizadeh, M., Harsij, M., 2024. Spatial and

temporal distribution of physicochemical parameters of water in Gorgan Bay (the southeast of the Caspian Sea-Iran): Fundamentals for the monitoring of the Caspian Sea coastal areas. *Marine Pollution Bulletin*, *201*, 116236.

Niroumand-Jadidi, M., Bovolo, F., 2021. Water quality retrieval and algal bloom detection using high-resolution CubeSat imagery. *ISPRS Annals of the Photogrammetry, Remote Sensing and Spatial Information Sciences*, *3*, pp.191-195.

Paerl, H.W., Huisman, J., 2009. Climate change: a catalyst for global expansion of harmful cyanobacterial blooms. *Environmental microbiology reports*, *1*(1), pp.27-37.

Pavelsky, T.M., Smith, L.C., 2009. Remote sensing of suspended sediment concentration, flow velocity, and lake recharge in the Peace-Athabasca Delta, Canada. *Water Resources Research*, *45*(11).

Peterson, K.T., Sagan, V., Sloan, J.J., 2020. Deep learning-based water quality estimation and anomaly detection using Landsat-8/Sentinel-2 virtual constellation and cloud computing. *GIScience & Remote Sensing*, *57*(4), pp.510-525.

Ranjbar, M.H., Hadjizadeh Zaker, N., 2016. Estimation of environmental capacity of phosphorus in Gorgan Bay, Iran, via a 3D ecological-hydrodynamic model. *Environmental monitoring and assessment*, *188*(11), p.649.

Rawat, K.S., Sahu, S.R., Singh, S.K., Chander, S., Gujrati, A., 2023. December: Water Quality Analysis Using Normalized Difference Chlorophyll Index (NDCI) and Normalized Difference Turbidity Index (NDTI), Using Google Earth Engine Platform. In *2023 International Conference on Modeling, Simulation & Intelligent Computing (MoSICom)* (pp. 408-413). IEEE.

Seenipandi, K., Ramachandran, K.K., Ghadei, P., Shekhar, S., 2021. Ocean remote sensing of suspended sediment variability in Southern Indian coastal water region using Landsat 8 OLI images. In *Remote Sensing of Ocean and Coastal Environments* (pp. 297-313). Elsevier.

Si, S., Zhang, H., Keerthi, S.S., Mahajan, D., Dhillon, I.S., Hsieh, C.J., 2017. Gradient boosted decision trees for high dimensional sparse output. In *International conference on machine learning* (pp. 3182-3190). PMLR (July 2017).

Sun, X., Zhang, Y., Shi, K., Zhang, Y., Li, N., Wang, W., Huang, X., Qin, B., 2022. Monitoring water quality using proximal remote sensing technology. *Science of the Total Environment*, *803*, p.149805.

Svirčev, Z., Simeunović, J., Subakov-Simić, G., Krstić, S., Pantelić, D., Dulić, T., 2013. Cyanobacterial blooms and their toxicity in Vojvodina lakes, Serbia. *International Journal of Environmental Research*, *7*(3), pp.745-758.

Topp, S.N., Pavelsky, T.M., Jensen, D., Simard, M., Ross, M.R., 2020. Research trends in the use of remote sensing for inland water quality science: Moving towards multidisciplinary applications. *Water*, *12*(1), p.169.

Wang, L., Xu, M., Liu, Y., Liu, H., Beck, R., Reif, M., Emery, E., Young, J., Wu, Q., 2020. Mapping freshwater chlorophyll-a concentrations at a regional scale integrating multi-sensor satellite observations with Google earth engine. *Remote Sensing*, *12*(20), p.3278.

Wu, C., Xie, M., Lin, L., He, S., Luo, C., Dong, H., 2025. A Study on Spatiotemporal Downscaling Methods for Chlorophyll-a Concentration in Taihu Lake Based on Remote Sensing Data from Sentinel-2 MSI and COMS-1 GOCI. *Water*, *17*(6), 855.

Yang, L., Driscol, J., Sarigai, S., Wu, Q., Lippitt, C.D., Morgan, M., 2022. Towards synoptic water monitoring systems: a review of AI methods for automating water body detection and water quality monitoring using remote sensing. *Sensors*, *22*(6), p.2416.

Zhao, M., O'Loughlin, F., 2025. A Multiplatform Approach for Chlorophyll Level Estimation for Irish Lakes. *IEEE Journal of Selected Topics in Applied Earth Observations and Remote Sensing*.